Aberration-Based Design Example for Freeform Optical Designs with Base Off-Axis Conics

Nick Takaki*[a,b], Aaron Bauer[a], Jannick P. Rolland[a]
[a]The Institute of Optics, University of Rochester, Rochester, NY, USA
[b]Synopsys, Inc., 11 Apex Drive, Marlborough, MA, USA 01752
*nicktakaki@gmail.com

ABSTRACT

A design method is shown that leverages the parameters of a base off-axis conic to eliminate the need for additional surface astigmatism and coma in freeform designs. A design example is given. Impact on testability estimates is discussed. © 2021 The Author(s)

Keywords: Optical design, freeform optics, off-axis conics, design for manufacturability and testability

1. INTRODUCTION

In this paper, we show, via a design example, how to leverage the parameters of a base off-axis conic to design freeform optical systems using the full-field display driven aberration-based design method discussed in [1].

Off-axis conic sections are often considered when designing unobscured or non-axisymmetric systems, including as base surfaces for freeform optics [2-8]. Likewise, design methods that use nodal aberration theory and full-field displays to gain insight into the aberrations of freeform systems have been demonstrated to be effective at generating starting points and performing designs (e.g., [1, 9-11]). However, in these aberration-based design methods, a central consideration is the correction of coma and astigmatism, which often involves the introduction of orthogonal polynomial astigmatism and coma terms (i.e.,, Z5/Z6 and Z7/Z8 for the Fringe Zernike polynomials). These terms are often major contributors to freeform departures, thus reducing or eliminating the need for orthogonal polynomial astigmatism and coma may improve interferometric testability estimates based on the magnitude of freeform departures.

Consequently, in this paper, we leverage the parameters of base off-axis conics to follow the aberration-based design method without the use of additional orthogonal polynomial astigmatism and coma terms. While an off-axis conic is not exactly equivalent to a sphere plus astigmatism and coma, it is shown via a design example that re-designing with base off-axis conic parameters from the start can yield a new design that achieves equivalent optical performance without orthogonal polynomial astigmatism and coma. When these design methods are coupled with design methods aimed at reducing surface departures, significant improvements in interferometric testability estimates can be achieved, including when compared to fitting freeform surfaces designed with base spheres with the best-fit off-axis conic after optimization.

For comparison, the design study in this paper is conducted twice: once using base off-axis conics with Fringe Zernike sag departure terms (excluding Zernike astigmatism and coma), and once using base spheres with Fringe Zernike sag departure terms (including Zernike astigmatism and coma).

2. FREEFORM SURFACES WITH BASE SPHERES AND OFF-AXIS CONICS

In this paper, freeform surfaces are characterized as a base surface plus freeform departures from that base surface. For example, a freeform surface with a base sphere and departures characterized with Fringe Zernike polynomials has a sag equation given as

$$z = f(\rho,\theta) = \frac{c\rho^2}{1+\sqrt{1-c^2\rho^2}} + \sum_j C_j Z_j(u,\theta),$$

International Optical Design Conference 2021, edited by Peter P. Clark, Richard N. Pfisterer, Henning Rehn, Simon Thibault, Proc. of SPIE Vol. 12078, 120781M · © 2021 SPIE · 0277-786X · doi: 10.1117/12.2603673

where $u = \rho/\rho_{\text{norm}}$ is the normalized radial coordinate and C_j is the coefficient of the j^{th} Fringe Zernike polynomial Z_j. When the base surface is null testable, the magnitude of the freeform departures can be used as an interferometric testability estimate [12-19]. While metrology is highly multidisciplinary and testability is more than just a number [20], reductions in freeform departures tend to facilitate improvements in interferometric testability when comparing designs that differ primarily in terms of freeform departures.

As noted above, the design methods in this paper leverage off-axis conic parameters to eliminate the need for additional Zernike astigmatism and coma. That is, if the sag equation of freeform surfaces with a base sphere plus Zernike departures is re-written as

$$z = f(\rho, \theta) = \text{Sag of Sphere} + Z5/\,Z6, Z7/\,Z8 + \text{Higher Order Terms},$$

then the sag of the freeform surfaces with base off-axis conics can be written as

$$z = f(\rho, \theta) = \text{Sag of OAC} + \text{Higher Order Terms}.$$

To characterize the sag of the off-axis conic, we use the parameterization initially discussed by Cardona-Nunez et al. and recently implemented in CODE V [21, 22]. The off-axis conic is parameterized via *R*, *k,* and ω, where *R* and *k* are the radius and conic constant of the parent surface, and ω is the offset angle formed by the parent surface's axis and off-axis segment's center surface normal. This parameterization grants smooth access to maximally off-axis ellipses, for which $\omega = 90°$.

Orthogonal polynomial sag departure is added to the base off-axis conic via use of the Zernike polynomials. As noted above, Zernike astigmatism and coma terms are not used with the base off-axis conic, which both facilitates reductions in freeform departures and breaks the degeneracy with the base off-axis conic parameters. It is expected that other orthogonal polynomial sag departure descriptions, such as 2D-Qs, could be used successfully as well, but examining this expectation is beyond the scope of this paper.

Following this construction and using tildes to denote the coordinates of the off-axis segment, the sag equation for freeform surfaces with base off-axis conics is given as [21]

$$z = f(\tilde{x}, \tilde{y}) = \frac{\gamma}{\beta + \sqrt{\beta^2 - \alpha\gamma}} + \sum_{j \neq 5,6,7,8} C_j Z_j(\tilde{u}, \tilde{\theta}),$$

where, as in [8], the terms $\alpha = \frac{1}{R}(1 + k\cos^2\omega), \beta = \frac{1}{\sqrt{1+k\sin^2\omega}} - \frac{k \sin\omega \cos\omega}{R}\tilde{y}, \gamma = \frac{1}{R}(\tilde{x}^2 + (1 + k\sin^2\omega)\tilde{y}^2)$ are calculated using Cardona-Nunez et al.'s approach but with a YZ-plane symmetric conic rather than the XZ-plane symmetric conic originally considered.

3. DESIGN EXAMPLE

We use a three-mirror LWIR telescope, originally designed by Fuerschbach et al. [9] and recently revisited by Takaki et al. [8, 23], as a design example. This design example is well-known in the literature, including assembly and testing [24], which makes it a useful example to revisit.

This design achieves an average RMS wavefront error over the field of 0.0085 waves at $\lambda = 10\ \mu m$, which is well below the diffraction limit. To facilitate comparison, we aim for roughly equivalent performance. A cross-section of the final design is shown in Figure 1, which has been reproduced from [8]. For full specifications, see Table 1, which has also been reproduced from [8].

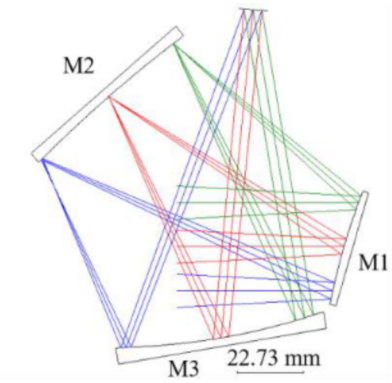

Figure 1. Cross-section of the final design, as originally shown in [8].

Table 1. Three-Mirror Telescope Specifications

Parameters	**Specifications**
Full Field-of-View (deg.)	8 × 6
Entrance Pupil Diameter (mm)	30
Focal Length (mm)	57
Average RMS WFE of Benchmark ($\lambda = 10$ μm)	0.0085 waves
Distortion (%)	< 3
Volume (ml)	< 820
Ball Geometry Radius (mm)	70

As noted in the introduction, two design processes are adopted and compared. The first design process adopts the aberration-based design method using spherical base surfaces and orthogonal polynomials to describe sag departures [1]. Full-field displays are used to identify aberrations, and orthogonal polynomial contributions are introduced to correct these aberrations. In the second design process, aberrations are still identified via full-field displays, but off-axis conic parameters are used to correct the initial limiting aberrations of the system, namely field-constant astigmatism and field-constant coma [2, 5-7].

Both designs use the same starting point, which has a similar layout and geometry as the final design but uses only spherical surfaces with no freeform contributions and therefore has virtually no aberration correction. A cross-section of the starting point design is shown in Figure 2.

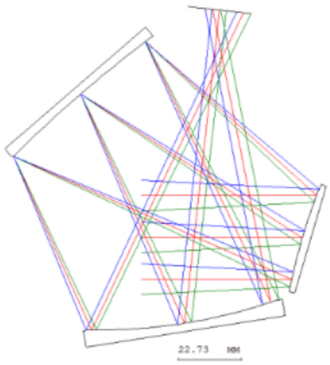

Figure 2. Cross-section of the starting point design. The design has the same layout and geometry as the final design but uses only spherical surfaces with no freeform contributions and has virtually no aberration correction.

Full-field displays, shown in Figure 3, are then used to analyze the initial limiting aberrations of this design. As a reminder, each symbol in a full-field display corresponds to a field-point, with the size and orientation of the symbol

corresponding to the magnitude and balance of the given aberration. As can be seen in Figure 3, the design is initially limited by 20 waves of field-constant astigmatism.

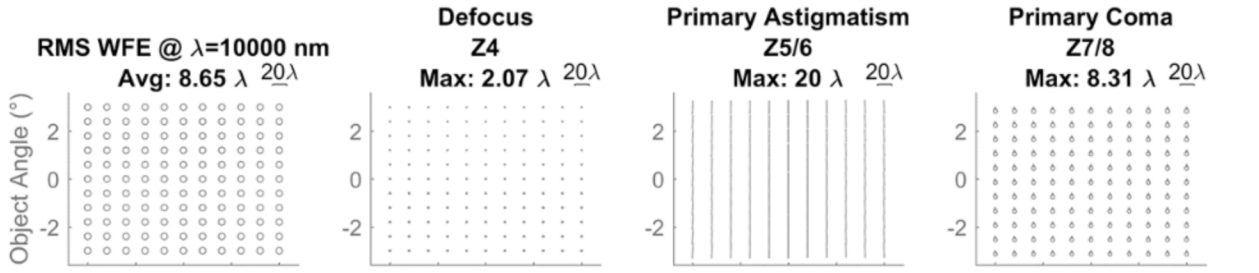

Figure 3. Full-field displays for the starting-point design. Note that the design is initially limited by twenty waves of field-constant astigmatism.

As noted by Fuerschbach et al., field-constant astigmatism can be corrected in the base sphere design by optimizing Zernike astigmatism terms, while leaving the power and geometry fixed. For the off-axis conic design, the goal is to achieve similar correction without the use of Zernike astigmatism. To facilitate this correction, we turn to maximally off-axis ellipses, for which the off-axis segment is located as far away from the axis of the parent as possible. As an example, consider the ellipse shown in Figure 4 below. For that ellipse, the segment in the blue square is centered on the major axis of the ellipse, which is also the axis of revolution used by an optical ellipse. On the other hand, the segment in the red square is centered maximally far away from this axis of revolution: if the red square were moved any further away, then it would get closer to the axis of revolution on the other side. As noted earlier in this presentation, maximally off-axis ellipses correspond to ellipses for which $\omega = 90°$.

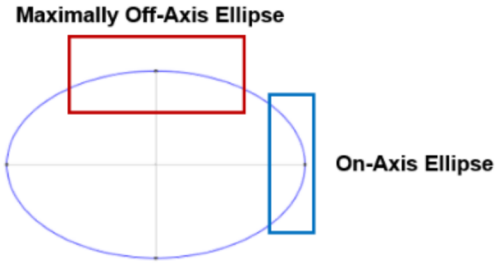

Figure 4. Maximally off-axis segments of ellipses for which $\omega = 90°$, versus on-axis ellipses for which $\omega = 0°$.

Maximally off-axis ellipses are fully plane symmetric (that is, are symmetric with respect to both the XZ and YZ plane) and differ from spheres primarily in terms of surface astigmatism (although other terms, such as surface spherical aberration, are also present). Importantly, because of this plane symmetry, maximally off-axis ellipses have no coma contributions. Consequently, to isolate and correct field-constant astigmatism, we require the use of maximally off-axis segments of ellipses by setting ω to 90°. We then constrain the geometry and off-axis conic power contributions (via the effective radius of curvature R_{eff}, defined in Schiesser et al. [25]), and then optimize both the conic constant k and radius of curvature R of the parent.

The full-field displays for astigmatism are shown for the base off-axis conic design and the base sphere design in Figure 5. While not exactly equivalent, comparable correction of field-constant astigmatism has been achieved. For the base off-axis conic design, only maximally off-axis ellipses are used to reduce field-constant astigmatism from 20 waves down to approximately 1.7 waves. For the base sphere design, Zernike astigmatism is used to fully correct the field-constant astigmatism (the node is slightly off-center to balance with other aberrations), leaving 3.7 waves of astigmatism remaining.

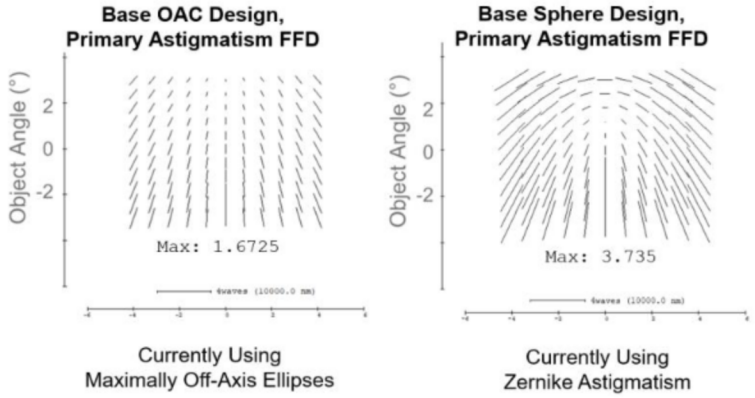

Figure 5. Full-field displays for astigmatism after correcting the initial field-constant astigmatism for the base off-axis conic design (left) and the base sphere design (right). Note that the correction is not exactly equivalent, but it is comparable. Note also that the base off-axis conic design only uses maximally off-axis ellipses, while the base sphere design uses Zernike astigmatism.

Next, the full-field displays are again examined: Figure 6 shows the full-field displays for the base off-axis conic design, with the base sphere design showing similar performance.

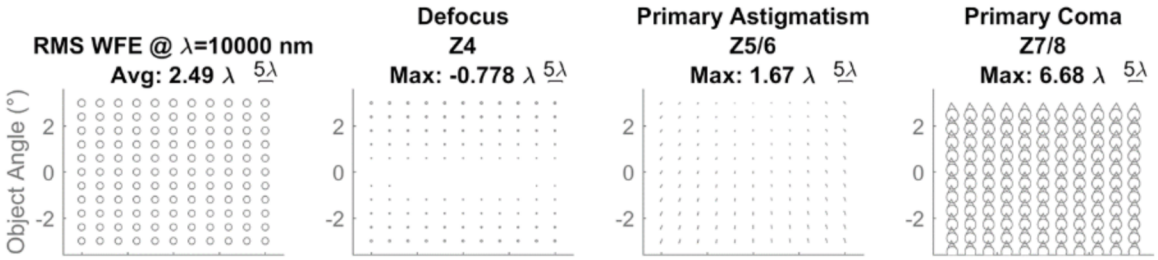

Figure 6. Full-field displays for the base off-axis conic design after correcting the initial field-constant astigmatism. Note that the limiting aberration is now field-constant coma, although field-asymmetric field-linear astigmatism can also be seen in Figure 5 above. The base sphere design yields similar performance (not shown).

For the base sphere design, the next step is to optimize Zernike coma at and away from the stop, which corrects both field-constant coma and field-asymmetric field-linear astigmatism. For the off-axis conic design, the segment's location is allowed to shift away from maximally off-axis (see Figure 7), while leaving the power of the base off-axis conic constrained. It is noted that that the parent conic no longer needs to be an ellipse, and the conic constant was constrained to be at most negative ten, to limit extreme hyperbolae.

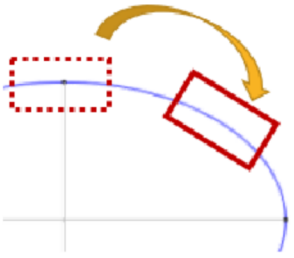

Figure 7. To correct field-constant coma and field-asymmetric field-linear astigmatism, the location of the off-axis segment is now allowed to deviate from maximally off-axis. This deviation is represented above with the shift from the maximally off-axis segment in dotted red lines to a non-maximal off-axis segment shown in solid red.

As with the correction of field-constant astigmatism, the correction of field-constant coma is not exactly equivalent between the two designs, but it is comparable. For the base off-axis conic design, only off-axis conic parameters have been leveraged, to achieve 0.7 waves of field-symmetric coma. For the base sphere design, Zernike astigmatism and

coma have been optimized to achieve 0.56 waves of field-symmetric coma. Full-field displays of coma are shown in Figure 8 below.

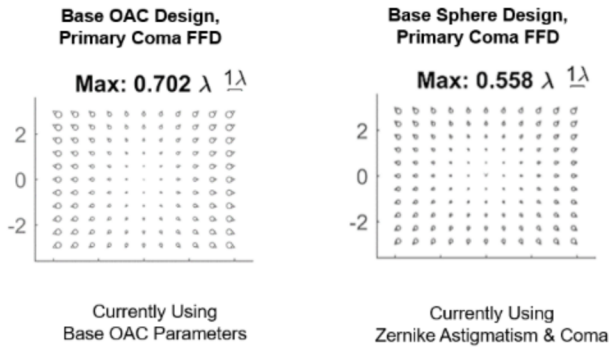

Figure 8. Full-field displays for coma for the base off-axis conic and base sphere designs after correcting field-constant coma. While the correction is not exactly equivalent, it is comparable. Note that the base off-axis conic design uses only base off-axis conic parameters for this correction, while the base sphere design uses Zernike astigmatism and coma terms.

At this point, the methods for the base off-axis conic design and the base sphere design are equivalent. In both cases, the next step is to introduce rotationally invariant Zernike terms (e.g., Z9 & Z16) to correct the field-symmetric aberrations. Later, when optimizing the power in the base sphere designs, we instead release the power constraints on the base off-axis conic. While it is noted that the base off-axis conics will have some rotationally invariant sag contributions relative to a base sphere, the three parameters for the off-axis conic have already been used to account for the surface power, astigmatism, and coma contributions. Zernike spherical aberration terms can thus be introduced to both designs.

Because the methods are equivalent moving forward from this stage of the design, we skip to the final design. Full-field displays of the RMS wavefront error are shown in Figure 9 below. Both designs achieve 0.006 waves of RMS wavefront error, which is below our target. Both designs also show approximately equivalent performance across the field.

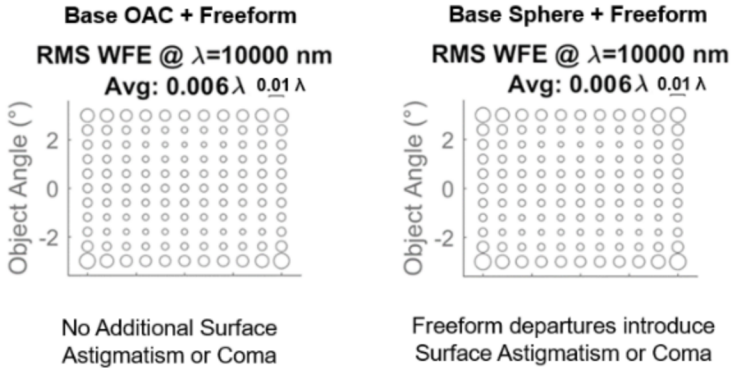

Figure 9. Full-field displays for the RMS wavefront error for the final designs. In both cases, optical performance is equivalent. Both designs achieve 0.006 waves of RMS wavefront error, with very similar field dependences. For the base off-axis conic design on the left, no additional Zernike astigmatism or coma has been used, although other Zernike terms are introduced. For the base sphere design, freeform departures include Zernike astigmatism and coma, as well as other Zernike terms.

4. REDUCED DEPARTURES IN DESIGNS WITH OFF-AXIS CONICS

The above result is interesting on its own, but its full impact is best demonstrated by combining the off-axis conic design methods discussed above with methods focused on improving surface testability estimates. Specifically, the square-sum penalty described in [23] is used in conjunction with use of up to the 36th Fringe Zernike term (although Zernike astigmatism and coma are still excluded for the base off-axis conic design), and testability estimates are examined at

intermediate points to prevent unnecessary sag departures from being introduced. This design approach is conducted for both the base off-axis conic design and the base sphere design.

The freeform departures, in terms of both PV sag departure and maximum gradient normal departure, are then examined for both the base sphere and base off-axis conic designs. For the base sphere design, departures are first reported relative to the best-fit sphere, and then relative to the best-fit off-axis conic. For the base off-axis conic design, departures are reported from the base off-axis conic. In all cases, departures are reported for each of the three mirrors individually and summed across all three mirrors. This sum is not a testability estimate in-and-of-itself, but it helps to verify that the overall testability estimates are improving, instead of being just shifted from one mirror onto another.

These testability estimates, which are shown in Table 2 below and visualized in the sag departure profiles in Figure 10, indicate that fitting an existing design with the best-fit off-axis conic yields some improvement in testability estimates, such as the improvement in PV sag departure from 225 μm to 54 μm for Mirror 3. However, fitting with the best-fit off-axis conic does not yield uniform improvement; Mirrors 1 and 2 show little change in PV sag departure, for example. On the other hand, re-designing with the base off-axis conic from the start yields new designs that have improvements in testability estimates by as much as an order of magnitude, even relative to fitting with the best-fit off-axis conic: the PV sag departure and maximum gradient normal departure improve from 54 μm and 0.41° to 5 μm and 0.07° for Mirror 3, with Mirrors 1 and 2 showing similar trends. The departures on the base off-axis conic design are potentially low enough to facilitate interferometric testing using conventional interferometers without additional null optics like computer-generated holograms, provided that the added complexity involved in nulling the base OAC can be overcome.

Please note that the results in this section have already been published in [8]. They are included because they demonstrate the impact of the design method proposed in this paper.

Table 2. Optical performance and testability estimates of (left) the base-sphere design with departures from best-fit sphere, (center) the base-sphere design with departures from best-fit off-axis conic, and (right) the base off-axis conic design with departures from the base off-axis conic.

Testability Estimates for the Three-Mirror Telescope Designs						
	Base Sphere + Zernikes Departures from Best-Fit Sphere		Base Sphere + Zernikes Departures from Best-Fit Off-Axis Conic		Off-Axis Conic + Zernikes Departures from Off-Axis Conic	
	Mean RMS WFE		Mean RMS WFE		Mean RMS WFE	
	0.0084 λ (λ = 10 μm)		0.0084 λ (λ = 10 μm)		0.0085 λ (λ = 10 μm)	
	PV Sag Departure	Max Gradient Normal Departure	PV Sag Departure	Max Gradient Normal Departure	PV Sag Departure	Max Gradient Normal Departure
M1	26 μm	0.25°	23 μm	0.35°	4 μm	0.05°
M2	9 μm	0.08°	8 μm	0.03°	3 μm	0.02°
M3	225 μm	0.68°	54 μm	0.41°	5 μm	0.07°
SUM	260 μm	1.01°	85 μm	0.79°	12 μm	0.14°

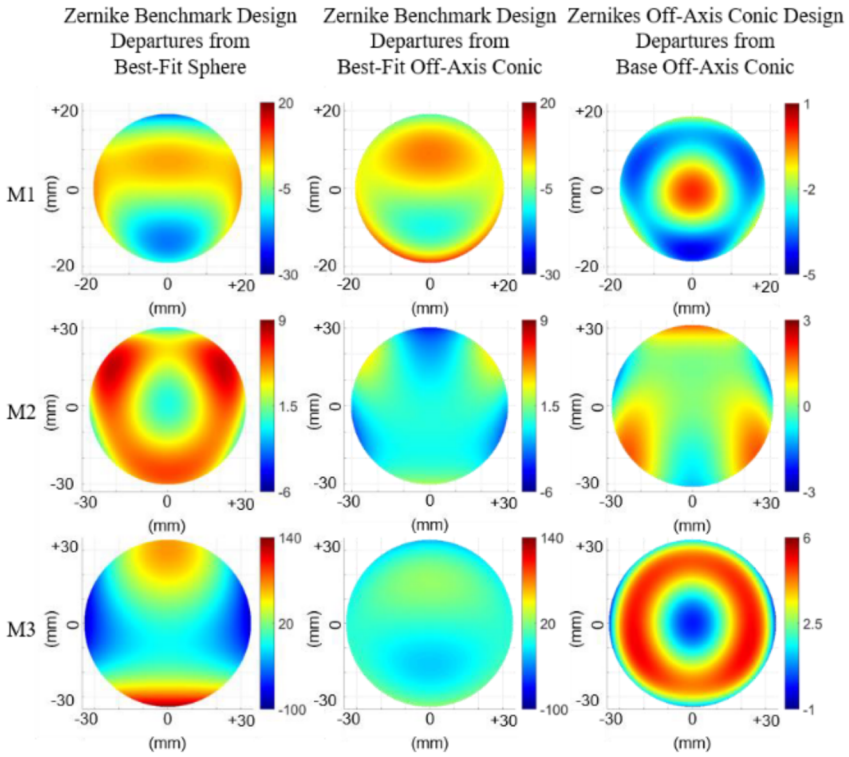

Figure 10. Sag departure profiles for: (left) the base sphere design with departures from best-fit sphere, (center) the base sphere design with departures from best-fit off-axis conic, and (right) the off-axis conic designs with departures from base off-axis conic. The scales of the color bars are in units of microns.

ACKNOWLEDGEMENTS

This research was supported by the National Science Foundation I/UCRC Center for Freeform Optics (IIP-1338877, IIP-1338898, IIP-1822049 and IIP-1822026).

REFERENCES

[1] A. Bauer, E. M. Schiesser, and J. P. Rolland, "Starting geometry creation and design method for freeform optics," Nature Communications **9**, 1756 (2018).

[2] J. Sasian, "How to approach the design of bilateral symmetric optical systems," Optical Engineering **33**, 2045-2061 (1994).

[3] S. Chang, "Linear astigmatism of confocal off-axis reflective imaging systems with N-conic mirrors and its elimination," J. Opt. Soc. Am. A **32**, 852-859 (2015).

[4] D. Reshidko and J. Sasian, "Method for the design of nonaxially symmetric optical systems using freeform surfaces," Optical Engineering **57**, 101704 (2018).

[5] J. Sasian, "The method of confocal mirror design," Proc. SPIE **10690**, 1069015 (2018).

[6] J. C. Papa, J. M. Howard, and J. P. Rolland, "Starting point designs for freeform four-mirror systems," Optical Engineering **57**, 101705 (2018).

[7] S. Chang, "A design method of linear-astigmatism-free three-mirror freeform imaging systems," in *Design and Fabrication Congress (Freeform, OFT)* (Optical Society of America, 2019),

[8] N. Takaki, J. C. Papa, A. Bauer, and J. P. Rolland, "Off-axis conics as base surfaces for freeform optics enable null testability," Optics Express **28**, 10859-10872 (2020).

[9] K. Fuerschbach, J. P. Rolland, and K. P. Thompson, "A new family of optical systems employing phi-type polynomial surfaces," Optics Express **19**, 21919-21928 (2011).

[10] K. Fuerschbach, J. P. Rolland, and K. P. Thompson, "Theory of aberration fields for general optical systems with freeform surfaces," Optics Express **22**, 26585-26606 (2014).
[11] J. P. Rolland, M. A. Davies, T. J. Suleski, C. J. Evans, A. Bauer, J. C. Lambropoulos, and K. Falaggis, "Freeform Optics for Imaging," Optica **8**, 161-176 (2021).
[12] J. Kumler, "Designing and specifying aspheres for manufacturability," Proc. SPIE **5874**, 58740C (2005).
[13] G. W. Forbes, "Manufacturability estimates for optical aspheres," Optics Express **19**, 9923-9942 (2011).
[14] F. Z. Fang, X. D. Zhang, A. Weckenmann, G. X. Zhang, and C. Evans, "Manufacturing and measurement of freeform optics," CIRP Annals **62**, 823-846 (2013).
[15] D. Stephenson and J. Kumler, "Optical design constraints for the successful fabrication and testing of aspheres," Proc. SPIE **9633**, 96330T (2015).
[16] T. Blalock, K. Medicus, and J. D. Nelson, "Fabrication of freeform optics," Proc. SPIE **9575**, 95750H (2015).
[17] T. Blalock, B. Myer, I. Ferralli, M. Brunelle, and T. Lynch, "Metrology for the manufacturing of freeform optics," Proc. SPIE **10448**, 1044817 (2017).
[18] J. Daniel, A. Sohn, and T. Devine, "Application of Freeform Aspheres to an Augmented Reality Technology Implementation " in *IODC 2017*, 2017), JW2C.3.
[19] M. A. Davies, Mechanical Engineering and Engineering Science, The University of North Carolina at Charlotte (personal communication, October 2, 2018).
[20] U. Fuchs and S. R. Kiontke, "Discussing design for manufacturability for two freeform imaging systems," Proc. SPIE **9948**, 99480L (2016).
[21] O. Cardona-Nunez, A. Cornejo-Rodriguez, R. Diaz-Uribe, A. Cordero-Davila, and J. Pedraza-Contreras, "Conic that best fits an off-axis conic section," Applied Optics **25**, 3585-3588 (1986).
[22] "Defining Special Surface Types," in *CODE V Lens System Setup Reference Manual* (Synopsys, Inc., 2019), pp. 241-314.
[23] N. Takaki, A. Bauer, and J. P. Rolland, "On-the-fly surface manufacturability constraints for freeform optical design enabled by orthogonal polynomials," Optics Express **27**, 6129-6146 (2019).
[24] K. Fuerschbach, K. P. Thompson, and J. P. Rolland, "Interferometric measurement of a concave, phi-polynomial Zernike mirror," Optics Letters **39**, 18-21 (2014).
[25] E. M. Schiesser, S.-W. Bahk, J. Bromage, and J. P. Rolland, "Gaussian curvature and stigmatic imaging relations for the design of an unobscured reflective relay," Optics Letters **43**, 4855-4858 (2018).